Theor Chem Acc (2000) 104:116–122
DOI 10.1007/s002140000114

Theoretical
Chemistry Accounts

Regular article

Plane-wave calculations applied to conjugated polymers

Geert Brocks

Computational Materials Science, Faculty of Applied Physics, University of Twente, P.O. Box 217, 7500 AE Enschede, The Netherlands

Received: 20 August 1999 / Accepted: 23 November 1999 / Published online: 19 April 2000

Abstract. Density functional calculations using pseudopotentials and a plane-wave basis set are applied to study the geometry and the electronic structure of conjugated polymers consisting of heterocyclic aromatic rings. This article focuses on the computational methods. The influence of the pseudopotentials on the structural and electronic properties is studied. The rates of convergence of these properties with respect to the basis set size and the density of sampling points for the Brillouin zone integration are considered. The effects of using different exchange–correlation potentials (local density or generalized gradient approximations) are examined. It is shown that smooth norm-conserving pseudopotentials used for calculations on conjugated polymers lead to converged results with a moderately sized basis set.

Key words: Conjugated polymer – Polythiophene – Density functional – Pseudopotential – Plane waves

1 Introduction

Density functional theory is the most widely used formalism in condensed matter physics to calculate electronic structures [1, 2]. Although computationally less demanding than Hartree–Fock calculations, all-electron density functional calculations on moderately sized systems can still be very time-consuming. A technique to reduce the computational effort and yet retain sufficient accuracy to describe the chemical bonding is to treat only the valence electrons explicity and to use pseudopotentials to represent the ion cores [3]. Pseudopotentials, although constructed for isolated atoms, are transferable to a molecular or solid-state environment [4]. Smooth pseudopotentials allow an expansion of the valence molecular orbitals in a plane-wave basis set of moderate size, which leads to compact mathematical expressions of the total energy and the Kohn–Sham equations in momentum space [5]. The local density approximation (LDA)/pseudopotential/plane-wave approach has become the principal technique in situations of low symmetry, such as surfaces and interfaces, in which a geometry optimization has to include many independent degrees of freedom [6]. The simultaneous optimization of electronic structure and geometry is widely used in the context of the Car–Parrinello scheme, which additionally allows one to combine an electronic structure calculation with classical molecular dynamics for the ion cores [7].

More recently Car–Parrinello calculations have been applied to condensed matter problems which traditionally have been outside the scope of solid-state physics, such as molecules in solution, molecular crystals and polymers [8–14]. A polymer crystal consists of polymer chains which have covalent bonding along the polymer chain; between polymer chains there is only van der Waals bonding. Conjugated polymers have received growing interest in recent years because of their intriguing optical and electronic properties, which has lead to novel electronic and electrooptical semiconductor devices [15]. We have used the LDA/pseudopotential/plane-wave technique to calculate and analyze the electronic structure of conjugated polymers [12, 16, 17]. With the help of such calculations promising structures for low-band-gap materials could be identified and practical design rules could be extracted [18–20]. More complex polymers are being considered at present for applications and these place stronger demands upon the computational efficiency of the techniques used to study their electronic structure.

This article is concerned with pseudopotential/plane-wave calculations on conjugated polymers and, in particular, with matters of computational efficiency. One of the standard problems associated with plane-wave basis sets is that convergence as a function of the basis set size can be notoriously slow, especially for first-row elements and 3*d* transition metals. The rate of convergence is intimately related to the smoothness of the pseudopotentials used. In Ref. [18] convergence was addressed for pseudopotentials fitted to an analytical form (and tabulated) by Bachelet, Hamann and Schlüter (BHS) for polyaminosquaraine [21]. Here the more flexible numerical pseudopotentials defined by Troullier and

Martins (TM) [22] are examined. Conjugated polymers which consist of heterocyclic aromatic rings are the simplest conjugated polymers that are of technological relevance; examples are shown in Fig. 1. Polythiophene (PTh) [16] is the primary test case. Nitrogen and oxygen are the first-row elements which are most difficult to handle with a plane-wave basis set [22]. Polyoxadiazole (POD) [17] is, therefore, the second test case. In systems which have translational symmetry, such as an ideal polymer chain, quantities such as the total energy are expressed as an integral over the first Brillouin zone (BZ) [23]. The accuracy of the numerical integration then determines the accuracy of those quantities. For semiconductors, usually a surprisingly small number of sampling points suffices for the numerical integration [24]. This is also the case for conjugated polymers, as will be illustrated for PTh and POD.

Most calculations use the "standard" local density functional which is based upon the numerical results of Ceperley and Alder [25, 26]. In recent years we have seen increased effort in constructing density functionals which, besides the local electron density, also depend on the gradient of the density [27]. Such generalized gradient approximations (GGA) foremost improve the calculated cohesive energies of molecules and solid state, which are too large when using the LDA. They have a smaller, though not necessarily positive, effect on structural energies, lattice constants and ionization potentials. Bulk moduli, vibration frequencies and intermolecular interactions even seem to become worse when using GGA [14, 28, 29]. The effects of gradient corrections on properties of conjugated polymers are tested using the Perdew–Wang functional (PW91) [30].

Section 2 briefly summarizes the theory that is used in the following sections, where the computational results are discussed. In the final section, the conclusions are summarized.

2 Theory

A basis set includes all plane waves $\exp(i\mathbf{G}_j \cdot \mathbf{r})$; $j = 1, \ldots, N$ with a wave vector of size $|\mathbf{G}_j|$ smaller than a cutoff value, usually presented in terms of a kinetic energy cutoff, E_{cut}.

$$\frac{\hbar^2 |\mathbf{G}_j|^2}{2m_e} \leq E_{\text{cut}} \quad , \tag{1}$$

where m_e is the electron mass. One uses periodic boundary conditions in all three spatial directions; the wave vectors, $\mathbf{G}_j$, satisfying Eq. (1) have to be commensurate with the periods. Equation (1) ensures uniform isotropic sampling of real space with a sampling density set by E_{cut}. The completeness of the basis set (and the real space sampling density) can be systematically improved by enlarging E_{cut}. One can mimic a single, isolated polymer chain by a unit cell which is sufficiently large in the directions perpendicular to the polymer chain such that the interaction between the periodic images is negligible. For a periodic system, convergence of the total energy is also controlled by the numerical accuracy of the BZ integration. For isolators/semiconductors the integrand can be expanded in a rapidly converging Fourier series, which implies that the integration can be performed using only a small number of sampling points in the BZ [24]. Convergence with respect to the BZ sampling density and convergence with respect to the plane-wave basis set size are usually independent [6, 18]. The minimum plane-wave basis set required to obtain meaningful results depends upon the particular pseudopotentials used. This can be understood by noting that the potential sets the typical length scale over which the valence wavefunctions vary strongly. This length scale needs to be sampled with sufficient density, which requires a sufficiently large E_{cut}.

Construction of an atomic pseudopotential starts by augmenting the rapidly varying all-electron valence functions, $\psi_{n,l}(r)$, $n = l + 1$, for each $l = 1, l_{\max}$ by a smooth monotonic function, $\phi_l(r)$, inside a core radius, $r_{c,l}$. The augmentation is done in a continuously differentiable way and, by construction, the functions $\psi_{l+1,l}(r)$ and $\phi_l(r)$ are identical for $r \geq r_{c,l}$. The pseudopotential terms, $V_l(r)$, are constructed by requiring that $\phi_l(r)$ are solutions of radial Kohn–Sham equations with $V_l(r)$ as potentials at the original all-electron eigenvalues $\epsilon_{n,l}, n = l + 1$ [4]. The augmentation procedure leaves considerable freedom for defining $\phi_l(r)$ and thus $V_l(r)$. As an example, Fig. 2 shows $V_l(r)$ and the corresponding

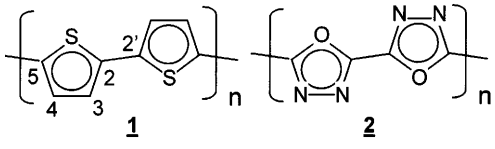

Fig. 1. Schematic structure of the polymers used as test cases for the calculations: polythiophene **1** and polyoxadiazole (*POD*) **2**

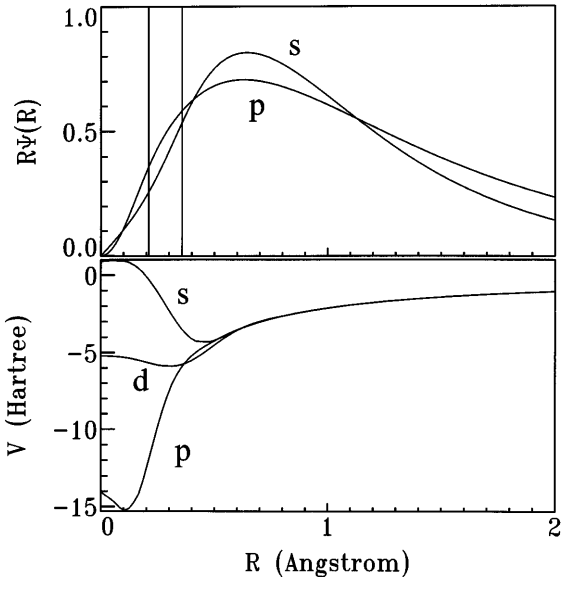

Fig. 2. Potential terms, $V_l(r)$, (*bottom*) and atomic pseudowavefunctions, $\phi_l(r)$, (*top*) of the Bachelet–Hamann–Schlüter (*BHS*) potential for carbon; *s, p* and *d* denote $l = 0,1,2$ terms. All terms coincide with $4/r$ at large r. The core radii, $r_{c,l}$, inside which the pseudowavefunctions deviate from the all-electron wavefunctions, are indicated by the *vertical lines*

$\phi_l(r)$ for carbon as given by BHS.[1] $V_l(r)$ have the same Z/r dependence at large r for all l (Z is the valence charge); they differ inside the region $r \le r_{c,l}$, the so-called core region. The full pseudopotential is

$$V(\mathbf{r}',\mathbf{r}) = \sum_{l,m=0,-l}^{\infty,l} Y^*_{l,m}(\hat{\mathbf{r}}')V_l(r)\delta(r'-r)Y_{l,m}(\hat{\mathbf{r}}) \ , \qquad (2)$$

where each $Y^*_{l,m}(\hat{\mathbf{r}}')Y_{l,m}(\hat{\mathbf{r}})$ term projects out one (l,m) component of the wave function on which the corresponding $V_l(r)$ operates. Making the approximation $V_l(r) = V_{l_{\max}}(r)$ for $l > l_{\max}$, where $l_{\max}$ denotes the lowest unoccupied subshell (e.g. $l_{\max} = 2$ for carbon), one obtains

$$V(\mathbf{r}',\mathbf{r}) = V_{l_{\max}}(r)\delta(\mathbf{r}'-\mathbf{r}) + \sum_{l,m=0,-l}^{l_{\max}-1,l} Y^*_{l,m}(\hat{\mathbf{r}}')\Delta V_l(r)\delta(r'-r)Y_{l,m}(\hat{\mathbf{r}}) \ , \qquad (3)$$

where $\Delta V_l(r) = V_l(r) - V_{l_{\max}}(r)$.[2] The second term on the right-hand side of Eq. (3) is a nonlocal and nonseparable potential, which makes it computationally demanding. It is more efficient to approximate it by a completely separable nonlocal (Hermitian) potential of the form $V_{\rm nl} = \sum_i a_i |\hat{A}\phi_i\rangle\langle\phi_i\hat{A}|$, with $|\phi_i\rangle = \phi_l(r)Y_{l,m}(\hat{\mathbf{r}})$ an atomic wave function. According to Kleinman and Bylander [31] the constants a_i and the operator $\hat{A}$ can be fixed by demanding that the potential of Eq. (3), with the last term replaced by $V_{\rm nl}$ operating on an atomic pseudo wavefunction $|\phi_i\rangle$, yields a result identical to that of the original potential. This gives $a_i = 1/\langle\phi_i|\hat{A}|\phi_i\rangle$ and $\hat{A} = \Delta V_l(r)$ and the final expression is

$$V(\mathbf{r}',\mathbf{r}) = V_{l_{\max}}(r)\delta(\mathbf{r}'-\mathbf{r}) + \sum_{l,m=0,-l}^{l_{\max}-1,l} \frac{Y^*_{l,m}(\hat{\mathbf{r}}')\phi^*_l(r')\Delta V_l(r')\Delta V_l(r)\phi_l(r)Y_{l,m}(\hat{\mathbf{r}})}{\int_0^\infty |\phi_l(r'')|^2 \Delta V_l(r'')r''^2 \mathrm{d}r''} . \qquad (4)$$

The last term on the right-hand side of Eq. (4) represents the nonlocal correction applied to components of the wave function with $l = 1$, $l_{\max} - 1$; the first term is a local potential applied to all l components. The nonlocal potential terms have a finite range, since all $V_l(r)$ terms have the same Z/r dependence at large r and thus $\Delta V_l(r) \longrightarrow 0$ at large r, cf. Fig. 2. For first- and second-row elements we use $l_{\max} = 2$, which means that the nonlocal part of the potential operates on the s and p parts of the wavefunctions.

3 Convergence results

In the first part of this section pseudopotential/plane-wave calculations are discussed based upon BHS pseudopotentials [21] and the LDA for exchange and correlation [25, 26]. More efficient pseudopotentials are introduced in Sect. 3.1. The effects of gradient corrections are considered in Sect. 3.2 using the (PW91) functional [30]. The primary test case is PTh. For carbon and sulphur BHS pseudopotentials are used; for hydrogen a purely local potential consisting of the s part of the BHS potential is used in all calculations. The unit cell has dimensions 7.833 Å along the PTh chain, which is the optimized lattice parameter, and 8 Å in the directions perpendicular to the polymer chain, which is sufficient to decouple the periodic images of the chain. With this unit cell $E_{\rm cut} = 30$ hartrees corresponds to about 13×10^3 plane waves.

A sufficient criterion for convergence with respect to the size of the plane-wave basis set is the total energy as a function of $E_{\rm cut}$; however, many relevant physical properties converge faster as a function of $E_{\rm cut}$ than the total energy, so the total energy is too strict a criterion. The cohesive energy, for instance, converges much faster than the total energy [6]. In the case of conjugated polymers, geometries and electronic structures are the most relevant physical properties, so these are used as convergence criteria. Optimized C—C bond lengths and the LDA band gap of PTh are shown in Fig. 3 as a function of $E_{\rm cut}$. Using $E_{\rm cut} = 30$ hartrees, the C—C bond lengths are converged within 0.005 Å and the LDA band gap within 0.01 eV. The C—S bond length is converged within 0.003 Å at $E_{\rm cut} = 20$ hartrees and the C—H bond length is particularly insensitive to the cutoff energy, so C—C bond lengths are the most critical parameters for the geometry here. Experiments usually yield larger errors for these quantities, implying that it does not make much sense to converge the calculations even further (actually even a smaller cutoff of 20 hartrees is acceptable in some cases). The BHS potential does not give a very uniform monotonic convergence as can be observed in Fig. 3; I will come back to this later.

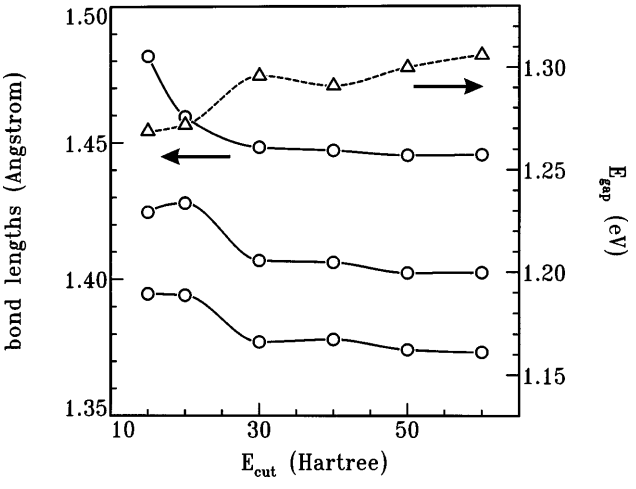

Fig. 3. Optimized C—C bond lengths (*circles*, *solid lines*) and local density approximation (*LDA*) band gap (*triangles*, *dashed line*) as function of basis set size. The *points* are calculated values; the *lines* are guides for the eye. The *lower three curves* correspond to (from *top* to *bottom*) the C2′—C2, C3—C4 and C2—C3 bond lengths respectively, cf. Fig. 1

[1] The BHS potential is expressed as $V_l(r) = V^{\rm BHS}_{\rm loc}(r) + V^{\rm BHS}_l(r)$, where the two terms on the right-hand side are tabulated, cf. Ref. [21]

[2] The unbound wavefunctions for high-l components show very little structure and $V_l(r)$ near the nucleus is dominated by the centrifugal kinetic energy, $l(l+1)/2m_e r^2$

As discussed in the previous section, the density of sampling points for BZ integration is the second important parameter for convergence. The C—C bond lengths and the LDA band gap are shown in Fig. 4 as a function of the number of BZ sampling points (k points). Since (by construction) the dispersion of the electronic bands perpendicular to the polymer chain is negligible, all sampling points can be placed along the polymer chain direction. In the following "n k points" refers to a one-dimensional equidistant grid of n points, centered at $k = 0$. Since convergence with respect to k-point sampling is independent of convergence with respect to cutoff, $E_{\text{cut}} = 20$ hartrees was used to obtain the results given in Fig. 4. Using three k points, the C—C bond lengths are converged within 0.003 Å and the gap within 0.05 eV; using two sampling points, the corresponding values are 0.01 Å and 0.1 eV, which in most cases is sufficiently accurate. As discussed in the previous section, such fast convergence as a function of the number of k points is typical for isolating and semiconducting materials. Comparing Figs. 3 and 4, we observe that the electronic band gap is relatively insensitive to E_{cut}, but is more sensitive to the number of k points. This difference is related to the interplay between the geometry and the band gap. More specifically the alternation between shorter and longer C—C bonds is closely connected to the size of the band gap; the larger the difference between short and long bonds, the larger the band gap [16]. Increasing the number of sampling points decreases this difference and thus decreases the band gap. Enlarging the cutoff only leads to a more or less uniform contraction of all bonds, which has a much smaller effect on the band gap.

According to the discussion in the previous section the rate of convergence with respect to E_{cut} is intimately connected to the pseudopotential. It is clear that the way in which the $V_l(r)$ terms are constructed in the core region ($r < r_{c,l}$) implicitly assumes that the core region is not important in describing the bonding properties of the atom. Naturally this can only be true if the core radii are chosen to be sufficiently small. Small core radii, however, result in hard pseudopotentials, i.e. potentials which vary strongly over a small (core) region. One needs plane waves with large wave vectors to expand the rapidly varying wavefunctions in such a core region; in other words one needs a large E_{cut}. The BHS potential for the p electrons of C, i.e. $V_{l=1}(r)$ in Fig. 2, is an example of a hard pseudopotential. The relatively slow convergence of the results shown in Fig. 3 reflects the hardness of (especially the p part of) this potential. However, within the constraints set by the scheme for constructing pseudopotentials (see the previous section) there remains considerable freedom to construct much smoother pseudopotentials.

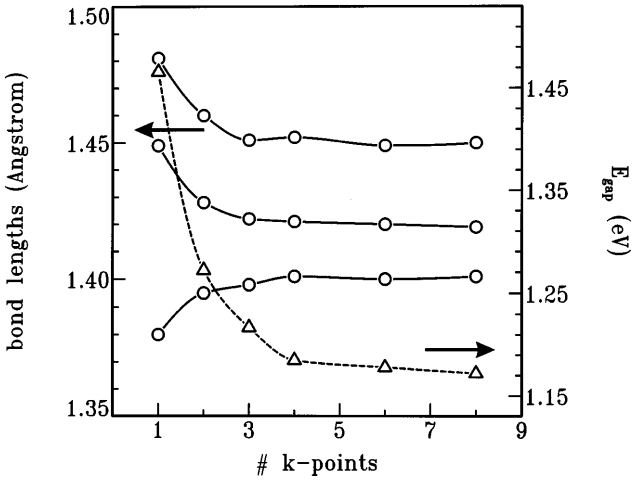

Fig. 4. As Fig. 3, but now as a function of the number of k-points used to sample the Brillouin zone

3.1 TM pseudopotentials

An algorithm for generating smooth pseudopotentials has been presented by Troullier and Martins [22]. I will use this algorithm to generate pseudopotentials based upon different values for the core radii and discuss convergence as a function of those core radii. Figure 5 shows two sets of $V_l(r)$ of TM potentials for carbon, the first set with $r_{c,l} = 0.56,\ 0.59,\ 0.59$ for $l = 0, 1, 2$, respectively (TM_1) and the second set with $r_{c,l} = 0.79, 0.81, 0.79$ Å (TM_2). In the first set the core radii are positioned just inside the outer maxima of the atomic pseudowavefunctions, as shown in Fig. 5 (dashed lines). In the second set the core radii are positioned just outside these maxima (solid lines). The C—C bond lengths in PTh are around 1.4 Å, which means that for the TM_1 potential the core radii do not overlap, whereas the TM_2 potential leads to an overlap of atomic core regions of about 0.2 Å. The latter seems to be in conflict with the demand that the core regions should not interfere with bonding properties, which is questionable

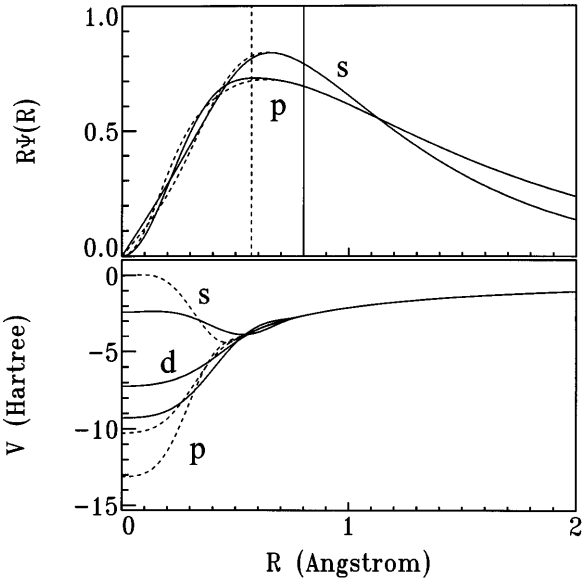

Fig. 5. $V_l(r)$ (*bottom*) and $\phi_l(r)$ (*top*) of Troullier–Martins (*TM*) potentials for carbon (cf. Fig. 2). The *dashed lines* refer to a potential generated with core radii near 0.6 Å; the *solid lines* refer to a potential generated with core radii near 0.8 Å

if these regions overlap. We will consider this in more detail below. Note for a start in Fig. 5 that the TM_2 potential leads to pseudowavefunctions that are almost indistinguishable up to about 0.2 Å inside its core radii from the wavefunctions generated with the TM_1 potential. This indicates that a small overlap of core regions can be tolerated. The effect of the core radii on the $V_l(r)$ terms is much more dramatic. The $V_l(r)$ coming from the larger core radii (TM_2) are much shallower and smoother than the ones coming from the smaller core radii (TM_1).

The convergence of C—C bond lengths and the LDA band gap as a function of E_{cut} for both the TM_1 and TM_2 potentials is shown in Fig. 6. The TM potential used for sulfur has $r_{c,l} = 0.94$ Å for $l = 0, 1, 2$; the C—S bond length is converged within 0.002 Å for $E_{\text{cut}} = 20$ hartrees, irrespective of the pseudopotential used for carbon, so again the C—C bond lengths are the more critical parameters. Comparing the results of Fig. 6 to the ones obtained with the BHS potential (Fig. 3), it is immediately observed that convergence is much more uniform for TM potentials. The overall convergence for the TM_1 potential (smaller core radii, dashed lines in Fig. 6) is comparable to the convergence obtained with the BHS potential: for $E_{\text{cut}} = 30$ hartrees the C—C bond lengths are converged within 0.001 Å and the LDA band gap within 0.007 eV. Using the TM_2 potential, the convergence as a function of cutoff energy is faster: with $E_{\text{cut}} = 20$ hartrees the C—C bond lengths are converged within 0.003 Å and the LDA band gap within 0.005 eV. This agrees with the notion that smoother potentials lead to faster convergence as a function of E_{cut}. Both the TM_1 and TM_2 potentials give similar converged results: their C—C bond lengths are within 0.002 Å and the LDA band gap is within 0.003 eV. This confirms the suggestion that the small overlap of atomic core regions which occurs in the TM_2 potential can be tolerated, since it does not affect the bonding in PTh. Since the smooth TM_2 potential leads to convergence at a much lower cutoff energy, it is to be preferred over the TM_1 and BHS potentials.

Enlarging the core radii gives even smoother potentials and thus faster convergence, but obviously this can lead to unphysical results. This is illustrated in Fig. 7, where converged C—C bond lengths and the LDA band gap are shown as a function of $r_{c,l}$. For $r_{c,l} > 0.8$ Å, the C—C bond lengths become unphysically small and also the LDA band gap starts to deteriorate. In conclusion, the core radii used for the TM_2 potential are optimal, since they give physically meaningful results at a moderately low cutoff energy. The small overlap of core regions of the TM_2 potential which occurs in the C—C bonding can be tolerated. This is related to the fact that whereas the construction of the TM pseudopotential only demands that pseudowavefunctions and all-electron atomic wavefunctions coincide for $r > r_{c,l}$, the smooth matching at $r = r_{c,l}$ in fact leads to a good coincidence also for slightly smaller r values [22] (cf. Fig. 5).

Although the discussion in the previous paragraph was centered around the TM potential for carbon, the conclusions are fairly general. This is illustrated by Fig. 8, where C—C, N—N, C—O and C—N bond lengths (in decreasing order) and the LDA band gap as a function of E_{cut} are shown for POD using BHS or TM potentials. The core radii used for the latter are $r_{c,l} = 0.76$ Å, $l = 0, 1, 2$ for nitrogen and $r_{c,l} = 0.73$ Å for oxygen. Bond lengths are converged within 0.001 Å and the LDA band gap within 0.01 eV using a cutoff energy of 30 hartrees. As before, reducing the core radii leads to the same converged values for the bond lengths (on a scale of 0.001 Å) and the LDA band gap (on a scale of 0.01 eV), but a higher cutoff energy is required in order to achieve convergence. Compared to the TM potentials, BHS potentials again give less uniform convergence, which is most clearly observed for the LDA band gap (the dashed line at the top of Fig. 8). Using $E_{\text{cut}} = 30$ hartrees with BHS potentials, the bond lengths are converged within 0.02 Å and the LDA band gap is converged within 0.1 eV. For some applications these

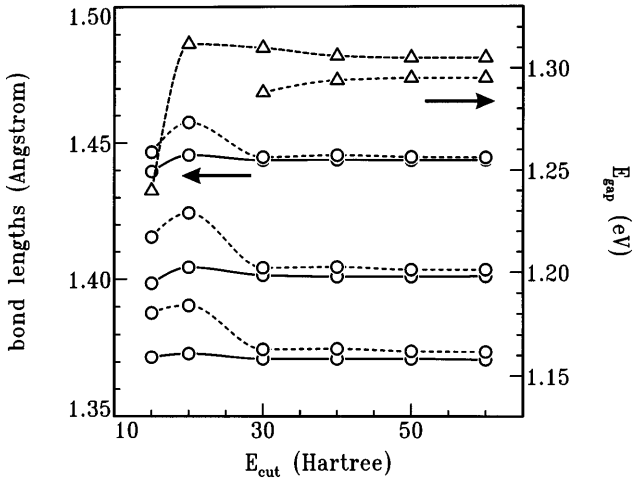

Fig. 6. As Fig. 3, but using the TM potentials as shown in Fig. 5. The *dotted lines* refer to results obtained using the potential generated with core radii near 0.6 Å; the *solid lines* refer to the potential generated with core radii near 0.8 Å

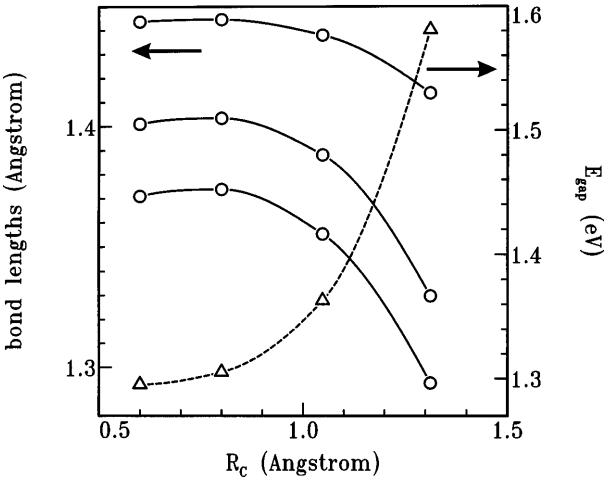

Fig. 7. Dependence of C—C bond lengths and LDA band gap on the core radii used to generate the TM pseudopotential

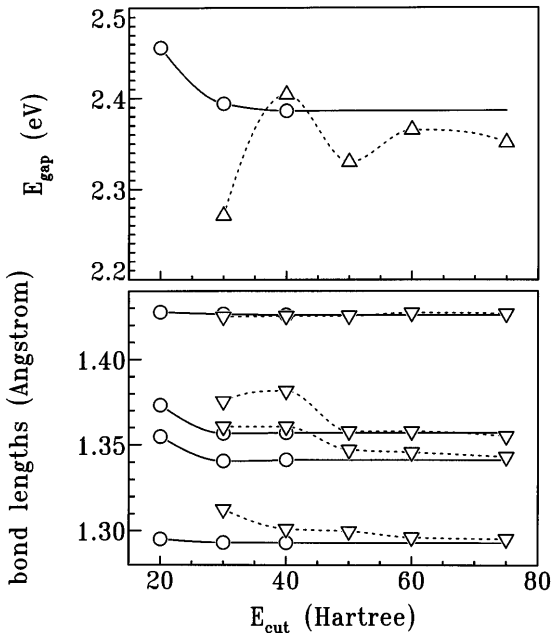

Fig. 8. Band gap (*top*) and bond lengths (*bottom*) for POD as a function of basis set size. The *circles* (*solid lines*) correspond to results obtained with TM potentials; the *triangles* (*dashed lines*) correspond to results obtained with BHS potentials. The bond length curves in the *lower figure* correspond to (from *top* to *bottom*) the C2′—C2, C—O, N—N and C—N bonds, respectively

convergence errors can be tolerated, but it will be clear that in general TM potentials are to be preferred.

3.2 Density functionals

In recent years, gradient corrected functionals of increased accuracy have become widely available [27, 30]. Replacing the standard LDA functional, these so-called GGA functionals foremost improve on the cohesive energies of molecules and crystals, which are severely overestimated within the LDA. GGA functionals have a much smaller, and not always positive, effect on other quantities, such as energy differences between molecular structures, lattice constants, vibration frequencies and ionization potentials [28, 29]. In this section the influence of a gradient-corrected functional on the structural properties of conjugated polymers is studied using the (PW91) functional [30] in calculations on PTh and POD. Naturally the exchange–correlation potential used in the atomic calculation in which the pseudopotential is generated has to be consistent with the exchange–correlation potential used in the molecular or solid-state calculation. Figure 9 shows a BHS-type pseudopotential generated using the GGA functional (PW91) in the atomic calculation. [3]One observes that this pseudopotential is nearly identical to the one generated with the LDA functional, except for the inner core region; this is consistent with previous calculations [29]. The effect which the GGA functional has on the optimized structures of PTh and POD is also quite small. Comparing the LDA and GGA generated structures, the bond lengths differ by less than 0.005 Å, bond angles differ in the order of 0.1° and the electronic band gap differs by 0.001 and 0.04 eV for PTh and POD, respectively. These calculations were done with a lattice constant which was fixed at the LDA optimized value. The difference between the optimized lattice constant using the GGA or the LDA functional is illustrated in Fig. 10 for POD. If the GGA functional is used, the optimized lattice constant is 6.789 Å, whereas for the

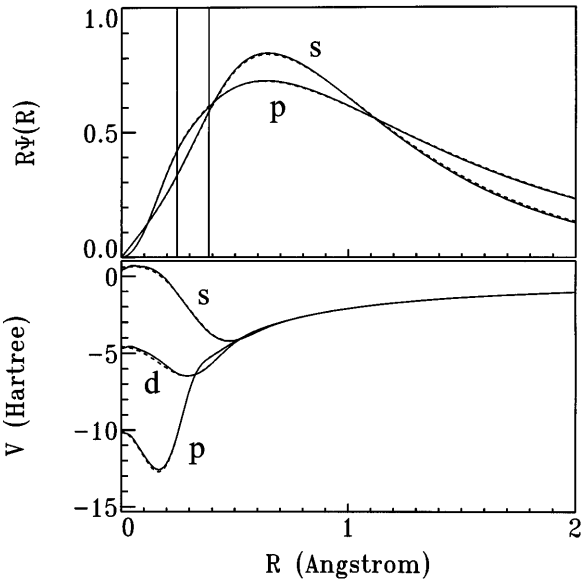

Fig. 9. BHS-type potentials generated using the generalized gradient approximation (*GGA*) (*solid lines*) and the LDA (*dashed lines*), respectively

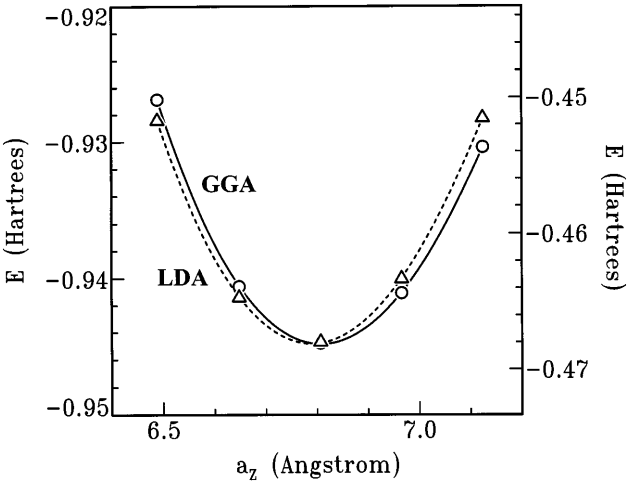

Fig. 10. Total energy, E, (in hartrees/unit cell) as a function of the lattice parameter, a_z, (in angstroms) for POD as calculated with the GGA functional (*solid line*; *left y-axis*) and the LDA functional (*dashed line*; *right y-axis*), respectively. Third-order polynomials are fitted through the point

[3]M. Fuchs, M. Bockstedte and M. Scheffler. Figure 9 shows BHS-type potentials with slightly different parameters, incorporating a nonlinear core correction

LDA functional it is 6.807 Å. The difference of less than 0.02 Å is negligible for most practical purposes. In conclusion, the calculated structural and electronic properties of polymers when using GGA or LDA functionals are very similar. The curvatures around the minimum of both curves in Fig. 10 differ by about 1%. This could be an indication that the GGA- or the LDA-generated bulk moduli and vibrational frequencies are also similar. Proof of this statement would, however, require a further detailed study.

Conclusions

Density functional calculations using pseudopotentials and a plane-wave basis set were applied to study the properties of conjugated polymers. A uniform convergence of geometry and electronic structure can be achieved using the flexible TM pseudopotentials. A small overlap of about 0.2 Å of atomic core regions can be tolerated when describing the chemical bonding, which means that converged results can be obtained for all first-row elements using $E_{\text{cut}} \approx 30$ hartrees; bond lengths are converged on a scale of 10^{-3}Å and band gaps on a scale of 10^{-2}eV. For carbon and second-row elements $E_{\text{cut}} \approx 20$ hartrees is sufficient to converge the results. Decreasing the atomic core regions requires a higher cutoff energy in order to get converged results. Increasing the core regions yields unphysical results for geometries and electronic structures. Convergence with respect to the number of sampling points used in the BZ integration is very fast. Three sampling points placed in the direction along the polymer backbone ensures convergence (for bond lengths within 5×10^{-3}Å and for the band gap within 5×10^{-2} eV), even two is sufficient for many purposes (bond lengths 10^{-2}Å, band gap 10^{-1} eV). On this scale the differences between the calculated structural and electronic properties of polymers when using GGA or LDA functionals are very small.

Acknowledgements. The author would like to thank J.L. Martins and M. Fuchs for making available their atomic pseudopotential programs. He acknowledges the financial support from Philips Research Laboratories through the Fundamenteel Onderzoek der Materie, Laboratorium zonder Muren program. The work was sponsored by the Stichting Nationale Computer Faciliteiten for the use of supercomputer facilities.

References

1. Kohn W, Sham LJ (1965) Phys Rev A 140: 1133
2. Jones RO, Gunnarson O (1989) Rev Mod Phys 61: 689
3. Heine V (1970) In: Ehrenreich H, Seitz F, Turnbull D (eds) Solid state physics, vol 24. Academic, New York
4. Hamann DR, Schlüter M, Chiang C (1979) Phys Rev Lett 43: 1494
5. Ihm J, Zunger A, Cohen ML (1979) J Phys C 12: 4409
6. Ramstad A, Brocks G, Kelly PJ (1995) Phys Rev B 51: 14504
7. Car R, Parrinello M (1985) Phys Rev Lett 55: 2471
8. Parrinello M (1997) Solid State Commun 102: 107
9. Molteni C, Parrinello M (1998) J Am Chem Soc 120: 2168
10. Brocks G (1997) Phys Rev B 55: 6816
11. Vogl P, Campbell DK (1990) Phys Rev B 41: 2797
12. Brocks G, Kelly PJ, Car R (1993) Synth Met 55–57: 4343
13. Blöchl PE, Togni A (1996) Organometallics 15: 4125
14. Milman V, Lee M-H (1996) J Phys Chem 100: 6093
15. Greenham NC, Friend R H (1995) In: Ehrenreich H, Spaepen F (eds) Solid state physics, vol 49. Academic, San Diego, p 63
16. (a) Brocks G (1996) J Phys Chem 100: 17327 (b) Brocks G (1997) J Phys Chem 101: 1264
17. Brocks G, Tol A (1997) J Chem Phys 106: 6418
18. Brocks G (1995) J Chem Phys 102: 2522
19. Brocks G, Tol A (1996) J Phys Chem 100: 1838
20. Brocks G, Tol A (1996) Synth Met 76: 213
21. Bachelet GB, Hamann DR, Schlüter M (1982) Phys Rev B 26: 4199
22. Troullier N, Martins JL (1991) Phys Rev B 43: 1993
23. Ashcroft NW, Mermin ND (1976) Solid state physics. Holt-Saunders, Philadelphia
24. Monkhorst HJ, Pack JD (1976) Phys Rev B 13: 5188
25. Ceperley DM, Alder BJ (1980) Phys Rev Lett 45: 566
26. Perdew J, Zunger A (1981) Phys Rev B 23: 5048
27. Burke K, Perdew JP, Ernzerhof M (1997) Int J Quantum Chem 61: 287
28. (a) Kutzler FW, Painter GS (1992) Phys Rev B 45: 3236; (b) García A, Elsässer C, Zhu J, Louie SG, Cohen ML (1992) Phys Rev B 46: 9829; (c) Perdew JP, Chevary JA, Vosko SH, Jackson KA, Pederson MR, Singh DJ, Fiolhais C (1992) Phys Rev B 46: 6671; (d) Dal Corso A, Pasquarello A, Baldereschi A, Car R (1996) Phys Rev B 53: 1180; (e) Andzelm J, Wimmer E (1993) J Chem Phys 96: 1280; (f) Johnson BC, Gill PMW, Pople JA (1993) J Chem Phys 98: 5612; (g) Fox T, Kollman PA (1996) J Phys Chem 100: 2950; (h) Trickey SB (1997) Int J Quantum Chem 61: 641; (i) Meijer E-J, Sprik M (1996) J Chem Phys 105: 8684
29. Hamann DR (1996) Phys Rev Lett 76: 660
30. (a) Perdew JP (1991) In: Ziesche P, Eschrig H (eds) Electronic structure of solids '91. Akademie Berlin (b) Perdew JP, Burke K, Ernzerhof M (1996) Phys Rev Lett 77: 3865
31. Kleinman L, Bylander DM (1982) Phys Rev Lett 48: 1425